Int J Adv Struct Eng (2015) 7:143–158
DOI 10.1007/s40091-015-0088-3

ORIGINAL RESEARCH

Boundary element analysis of post-tensioned slabs

Youssef F. Rashed[1,2]

Received: 10 June 2014 / Accepted: 6 April 2015 / Published online: 1 May 2015

Abstract In this paper, the boundary element method is applied to carry out the structural analysis of post-tensioned flat slabs. The shear-deformable plate-bending model is employed. The effect of the pre-stressing cables is taken into account via the equivalent load method. The formulation is automated using a computer program, which uses quadratic boundary elements. Verification samples are presented, and finally a practical application is analyzed where results are compared against those obtained from the finite element method. The proposed method is efficient in terms of computer storage and processing time as well as the ease in data input and modifications.

Keywords Post-tensioned slabs · Boundary element method · Equivalent load method

Introduction

Flat slabs are desirable structural systems in engineering due to architectural needs and speed of construction. In order to construct flat slabs with large spans (about 12–15 m), pre-stressing cables are necessary (Post tensioning manual 2000). Several finite element method (FEM) (Zienkiewicz 1977) based packages are used to carry out the structural analysis of plate structures; among them are the SAP2000 (2006) and SAFE (2008), etc. However, special packages are designed to treat the presence of post-tensioned cables such as ADAPT (2007) and SAFE-PT (2008). All of these packages, no exception, are based on the finite element method.

The boundary element method (BEM) (Berrebia et al. 1984) has emerged as a powerful tool in engineering practice. The BEM for thin plates started with the work of Bézine (1978) and Stern (1979) for the direct formulation and by Tottenham (1979) for the indirect formulation. Van der Weeën (1982) was the first who applied the boundary element method to shear-deformable plate-bending problems according to Reissner (1947). Rashed (2005a, b) extended formulation of Van der Weeën (1982) to model flat plates over columns. It was presented in Ref. (Rashed 2005a, b; Nazief et al. 2010) that the Reissner plate-bending model is more refined and accurate in theory for thin slabs and thick foundation plates. To the author's best knowledge, none of these publications considered the presence of pre-stressing cables in flat slabs.

This paper aims to include the effect of post-tensioning cables within the boundary element formulation for flat slabs. It can be regarded as a new structural analysis tool for post-tensioned slabs. Unlike previous technology, which is mainly based on the FEM, the proposed method is based on the boundary element method. This will avoid any internal meshing problems and will guarantee high accuracy for both slabs and supporting elements. The proposed method is easy in data input and modifications. It is also fast in computer processing time and has less storage requirements. Therefore, practical projects results could be sent easily by e-mail. Cables are placed freely inside the slab with no meshing constraints, which provides robust tool for optimization and value engineering. Results of the proposed model are compared against those obtained from the FEM. This comparison proved the validity of the present formulation.

✉ Youssef F. Rashed
yrashed@hotmail.com; yrashed@eng.cu.edu.eg

[1] Supreme Council of Universities, Giza, Egypt

[2] Department of Structural Engineering, Cairo University, Giza, Egypt

Boundary elements for flat slabs

Consider the slab shown in Fig. 1. According to Rashed (2005a, b) columns or internal walls are modeled using internal supporting cells with the real geometry of their cross sections. This ensures avoiding overshooting stress resultant values over supports. Three generalized forces are considered at each internal support: two bending moments in the two spatial directions (x_1, x_2) as well as a shear force in the vertical direction (x_3). These generalized forces are considered to vary constantly over the column cross section (Rashed 2005a, b). A suitable boundary integral equation (in index form) can be written as follows (Rashed 2005a, b):

$$C_{ij}(\xi)u_j(\xi)+\int_{\Gamma(x)} T_{ij}(\xi,x)u_j(x)\mathrm{d}\Gamma(x)=\int_{\Gamma(x)} U_{ij}(\xi,x)t_j(x)\mathrm{d}\Gamma(x)$$
$$+\int_{\Gamma(x)}\left[V_{i,n}(\xi,x)-\frac{v}{(1-v)\lambda^2}U_{i\alpha}(\xi,x)\right]q\,\mathrm{d}\Gamma(x)$$
$$+\sum_{\text{columns}(C)}\left\{\int_{\Omega_C(y)}\left[U_{ik}(\xi,y)-\frac{v}{(1-v)\lambda^2}U_{i\alpha,\alpha}(\xi,y)\delta_{3k}\right]\mathrm{d}\Omega_C(y)\right\}$$
$$\times\left[\frac{-u_k(y)S_k(y)}{A(y)}-q\delta_{3k}B(y)\right]. \quad (1)$$

where $U_{ij}(\xi,x)$ and $T_{ij}(\xi,x)$ are the fundamental solution kernels (Vander Weeën 1982), $u_j(x)$, $t_j(x)$ are the boundary displacements and tractions, $C_{ij}(\xi)$ is the jump term at the source point, ξ (= ½ for ξ on smooth boundary), $\Omega_C(y)$ denotes the column's y domain, y is a field point at the column center, $S_k(y)$ is the column's y stiffness, $A(y)$ is the column's y area, q is the uniform domain loading and $B(y)$ is a coefficient (equal to zero in case column stops below the considered floor and equal to one in case column continues above the considered floor). It has to be noted that long walls and cores can be treated as column segments. Beams can be also modeled in similar way but using special stiffness matrix. In order to solve the problem in Eq. (1), additional collocation scheme is carried out at each column center. In this case additional three integral equations similar to that of Eq. (1) could be written but with: $\xi = y$ and $C_{ij}(y) = 1$. These new equations together with Eq. (1) can solve the boundary value problem (Rashed 2005a, b).

After the boundary solution, values of the displacement and forces at column centers are also calculated. Generalized displacements at the internal point ξ can be obtained using Eq. (1) with $C_{ij}(y) = 1$. The stress resultants at the internal point ξ are obtained as follows (Rashed 2005a, b):

$$M_{\alpha\beta}(\xi)=\int_{\Gamma(x)} U_{\alpha\beta k}(\xi,x)t_k(x)\mathrm{d}\Gamma(x)-\int_{\Gamma(x)} T_{\alpha\beta k}(\xi,x)u_k(x)\mathrm{d}\Gamma(x)$$
$$+q\int_{\Gamma(x)} W_{\alpha\beta}(\xi,x)\mathrm{d}\Gamma(x)+\frac{v}{(1-v)\lambda^2}q\delta_{\alpha\beta}$$
$$+\sum_{\text{columns}(C)}\left\{\int_{\Omega_C(y)}\left[U_{\alpha\beta k}(\xi,y)-\frac{v}{(1-v)\lambda^2}U_{\alpha\beta\theta,\theta}(\xi,y)\delta_{3k}\right]\mathrm{d}\Omega_C(y)\right\}$$
$$\times\left[\frac{-u_k(y)S_k(y)}{A(y)}-q\delta_{3k}B(y)\right] \quad (2)$$

$$Q_{3\beta}(\xi)=\int_{\Gamma(x)} U_{3\beta k}(\xi,x)t_k(x)\mathrm{d}\Gamma(x)$$
$$-\int_{\Gamma(x)} T_{3\beta k}(\xi,x)u_k(x)\mathrm{d}\Gamma(x)+q\int_{\Gamma(x)} W_{3\beta}(\xi,x)\mathrm{d}\Gamma(x)$$
$$+\sum_{\text{columns}(C)}\left\{\int_{\Omega_C(y)}\left[U_{3\beta k}(\xi,y)-\frac{v}{(1-v)\lambda^2}U_{3\beta\theta,\theta}(\xi,y)\delta_{3k}\right]\mathrm{d}\Omega_C(y)\right\}$$
$$\times\left[\frac{-u_k(y)S_k(y)}{A(y)}-q\delta_{3k}B(y)\right] \quad (3)$$

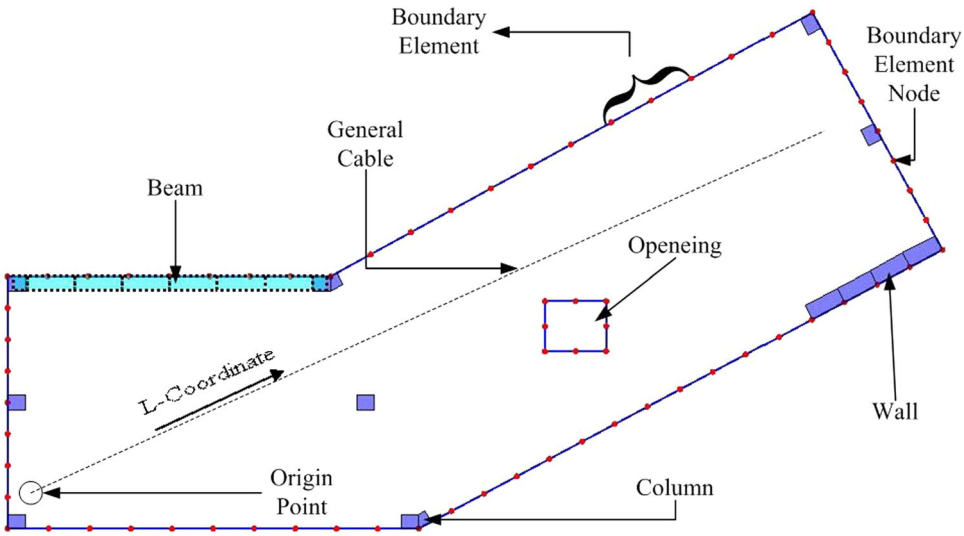

Fig. 1 A general post-tensioned slab problem

where the new kernels $U_{ijk}(\xi,x)$ and $T_{ijk}(\xi,x)$ are given in Vander Weeën (1982).

Proposed model for pre-stressing cables

In this section, the pre-stressing cables are introduced to the boundary element formulation presented in Sect. 3 using the equivalent load method (Lin 1963).

The equivalent load method

Consider a general cable profile shown in Fig. 2. This profile can be represented in terms of the following parabolic equation:

$$Z(L) = a_1 L^2 + a_2 L + a_3 \tag{4}$$

where, a_1, a_2, and a_3 are constants to be determined from the cable boundary conditions. The coordinate L is measured from an arbitrary origin (see Fig. 1) along the cable and Z is the cable eccentricity in the x_3 direction measured from slab centerline (see Fig. 2).

The derivatives of Eq. (4) w.r.t. the coordinate L are:

$$Z'(L) = 2a_1 L + a_2 \tag{5}$$

$$Z''(L) = 2a_1. \tag{6}$$

Equivalent cable loads on each segment are represented (Lin 1963) by distributed load (W) along the cable length together with two concentrated forces ($F_3(L_s)$, $F_3(L_e)$) and two concentrated moments ($F_\alpha(L_s)$, $F_\alpha(L_e)$) at the segment start (L_s) and end (L_e) points (see Fig. 2). Equivalent distributed load is computed as follows (Lin 1963):

$$W = P\,Z'' = P(2a_1) \tag{7}$$

Concentrated load values are computed as follows (Lin 1963):

$$F_3(L_s) = PZ'(L_s) = P(2a_1 L_s + a_2) \tag{8}$$

$$F_3(L_e) = PZ'(L_e) = P(2a_1 L_e + a_2) \tag{9}$$

where, P is the pre-stressing force of the considered cable.

Concentrated moment values due to the cable eccentricity are computed as follows (Lin 1963):

$$F_a(L_s) = PZ(L_s) \tag{10}$$

$$F_a(L_e) = PZ(L_e) \tag{11}$$

where the α-direction is the perpendicular to the L-direction and the right hand vector notation is used to represent the bending moment. The $F_a(L_s)$ and $F_a(L_e)$ is going to be resolved into: $F_1(L_s)$, $F_1(L_e)$ and $F_2(L_s)$, $F_2(L_e)$ in the x_1 and x_2 directions.

If cable profile has any local change in curvature, two segments are used to model this cable. Hence, additional concentrated load is added at the point of discontinuity, with a value equal to the summation of end concentrated loads for the two intersecting segments. Moreover, equivalent load for any continuous cable having variable segment profiles is calculated by dividing the cable into series of parabolic segments.

Boundary element implementations

In the boundary element model, each cable is divided into series of patch loading cells [n cells with centers located at

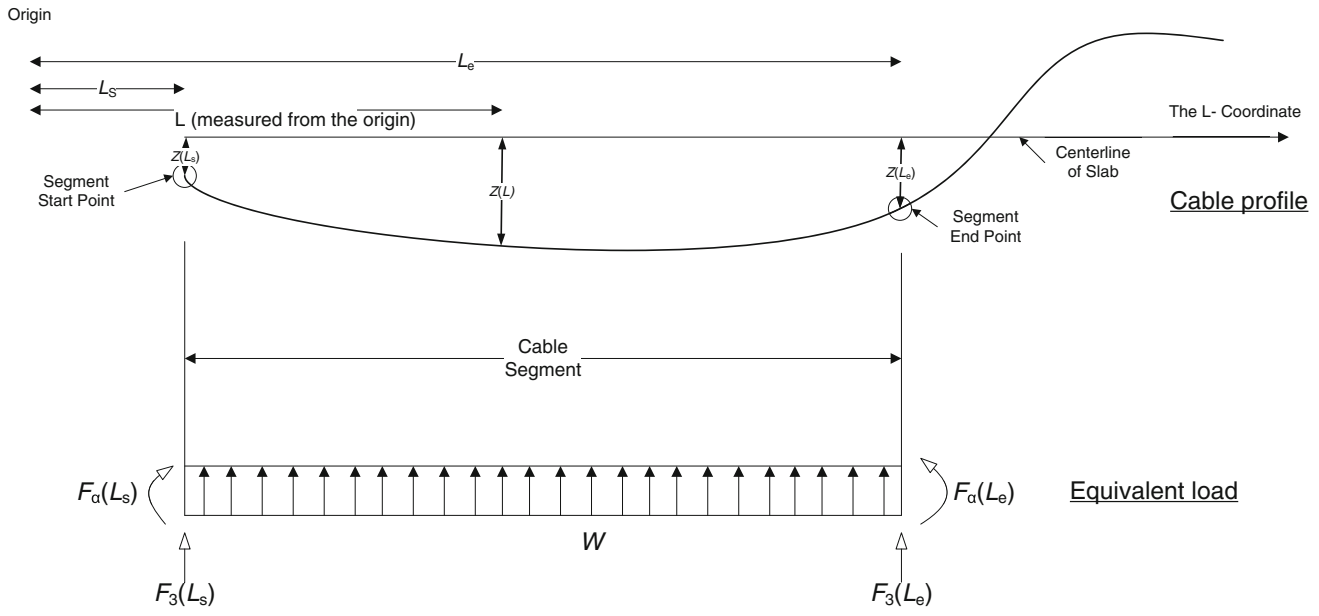

Fig. 2 Elevation view showing the equivalent load for a general cable segment

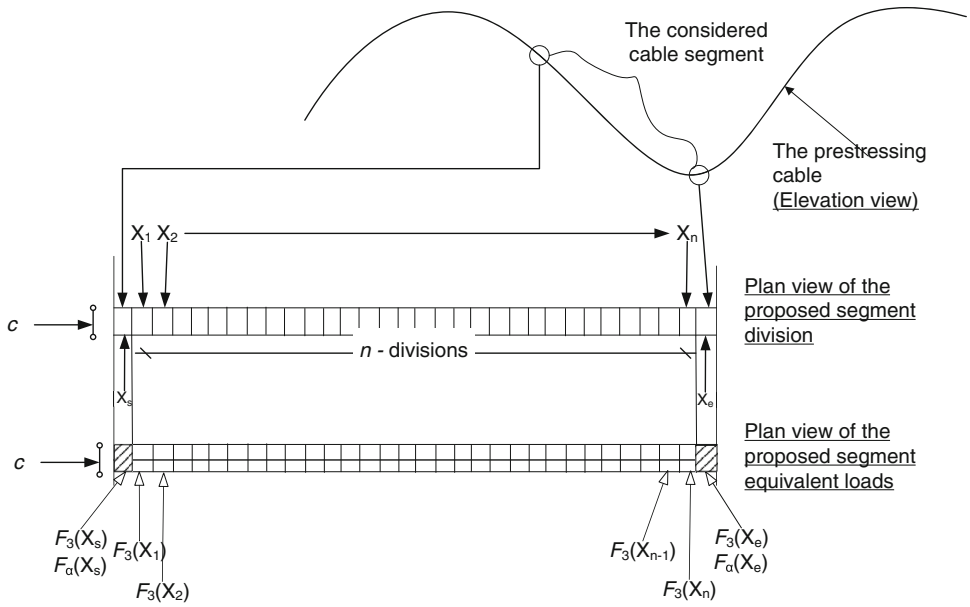

Fig. 3 The proposed boundary element modeling of the cable segment equivalent loads

$(X_1, X_2 \ldots X_n)$ as shown in Fig. 3] to model the distributed load (W). The width of these cells is equal to the cable width (c). The locations of such points could be obtained easily using simple geometry relationships. Additional two square cells (of dimensions equal to $c \times c$) are placed at the beginning ($X_s = X_s(L_s)$ and at the end ($X_e = X_e(L_e)$) of each cable to represent the concentrated loads (F_3) and moments (F_α). In order to account for such new cable loading additional terms have to be added to right hand side of the boundary integral Eq. (1) as follows:

$$+\sum_{\text{cables}}\left[\sum_{N=1}^{n}F_3^*(X_N)\int_{\Omega(X_N)}\left[U_{i3}(\xi,X_N)-\frac{v}{(1-v)\lambda^2}U_{i\alpha,\alpha}(\xi,X_N)\right]d\Omega(X_N)\right]$$
$$+\sum_{Q=\text{s,e}}F_j^*(X_Q)\int_{\Omega(X_Q)}\left[U_{ij}(\xi,X_Q)-\frac{v}{(1-v)\lambda^2}U_{i\alpha,\alpha}(\xi,X_Q)\delta_{3j}\right]\mathrm{d}\Omega(X_Q) \tag{12}$$

In addition, the following additional terms have to be added to the right hand side of Eq. (2) for the moment calculations:

$$+\sum_{\text{cables}}\left[\sum_{N=1}^{n}F_3^*(X_N)\int_{\Omega(X_N)}\left[U_{\alpha\beta3}(\xi,X_N)-\frac{v}{(1-v)\lambda^2}U_{\alpha\beta\theta,\theta}(\xi,X_N)\right]\mathrm{d}\Omega(X_N)\right]$$
$$+\sum_{Q=\text{s,e}}F_k^*(X_Q)\int_{\Omega(X_Q)}\left[U_{\alpha\beta k}(\xi,X_Q)-\frac{v}{(1-v)\lambda^2}U_{\alpha\beta\theta,\theta}(\xi,X_Q)\delta_{3k}\right]d\Omega(X_Q) \tag{13}$$

and the following terms have to be added to the right hand side of Eq. (3) for the shear calculations:

$$+\sum_{\text{cables}}\left[\sum_{N=1}^{n}F_3^*(X_N)\int_{\Omega(X_N)}\left[U_{3\beta3}(\xi,X_N)-\frac{v}{(1-v)\lambda^2}U_{3\beta\theta,\theta}(\xi,X_N)\right]\mathrm{d}\Omega(X_N)\right]$$
$$+\sum_{Q=\text{s,e}}F_k^*(X_Q)\int_{\Omega(X_Q)}\left[U_{3\beta k}(\xi,X_Q)-\frac{v}{(1-v)\lambda^2}U_{3\beta\theta,\theta}(\xi,X_Q)\delta_{3k}\right]\mathrm{d}\Omega(X_Q) \tag{14}$$

where, X_N is the center point of the subdivision number N (see Fig. 3), X_S, X_e are the start and the end points of the cable segment, respectively, $F_3^*(X_N)$ is the vertical pressure for subdivision number N, and $F_k^*(X_Q)$ is the moment per unit area when $k = 1, 2$ and it represents the vertical pressure $\left(F_3^*\right)$ when $k = 3$. Values of F_k^* can be obtained as follows:

$$F_k^*(\mathrm{X}_Q) = F_k(\mathrm{X}_Q)/c^2 \tag{15}$$

and

$$F_3^*(\mathrm{X}_N) = F_3(\mathrm{X}_N)\Big/\left[\frac{\ell_{\text{cable}}}{n}\times c\right] \tag{16}$$

in which ℓ_{cable} is the horizontal distant from X_s to X_e.

Similar to Eqs. 1, 2 and 3 in Sect. 3, it has to be notes that in Eq. (12) ξ has to be collocated at all boundary points plus at internal columns and walls centers as well as at beam cell centers. Whereas, in Eqs. (13) and (14), ξ has to be any internal point.

Numerical implementations

The previous boundary element formulation is implemented into computer code using quadratic boundary

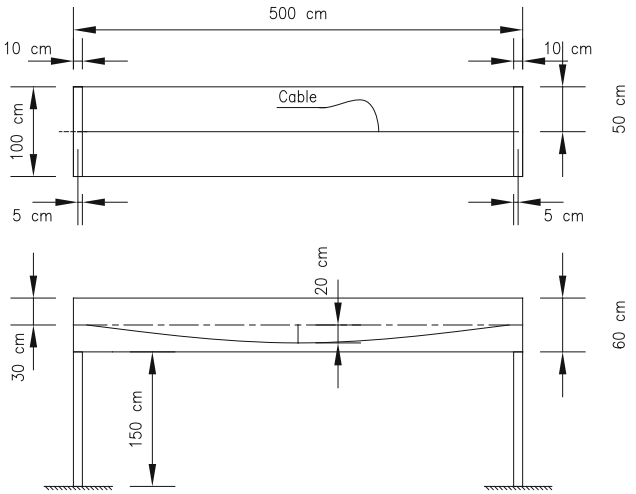

Fig. 4 The simply supported slab considered in Sect. 4.1

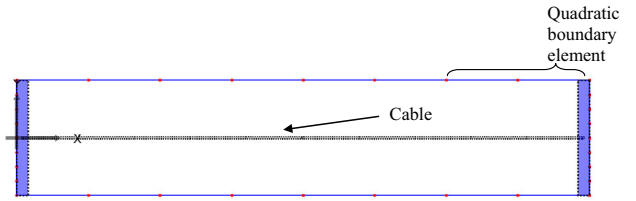

Fig. 5 Boundary element and cable internal cells for the simply supported slab considered in Sect. 4.1

elements. This code is called the PLPAK. Two main software tools are implemented to add the effect of the prestressing cables. The first tool is called the "Cable Calculator", which allows inputting the cable data using different formats and determine the constants a_1, a_2 and a_3 from the cable geometry (recall Sect. 3.1). The second tool is the "PTUpdater" which changes the cable data into equivalent load as described in Sect. 3.1. It also updates the boundary element model with such equivalent loads as demonstrated in Sect. 3.2. Hence, the traditional steps of solution for boundary elements are carried out (SAP2000 2006).

Numerical verifications

The purpose of this section is to verify the proposed formulation presented in Sect. 3 for simple problems where analytical solutions are existed in the literature.

Load balancing of simply-supported slab own weight

In this example, the slab shown in Fig. 4 is considered. The slab has cross-section dimensions of 1.0×0.6 m. The material properties taken are $E = 2.21 \times 10^6$ t/m^2, $\upsilon = 0$ to allow comparison against results for the beam theory. The slab is pre-stressed with one cable of force

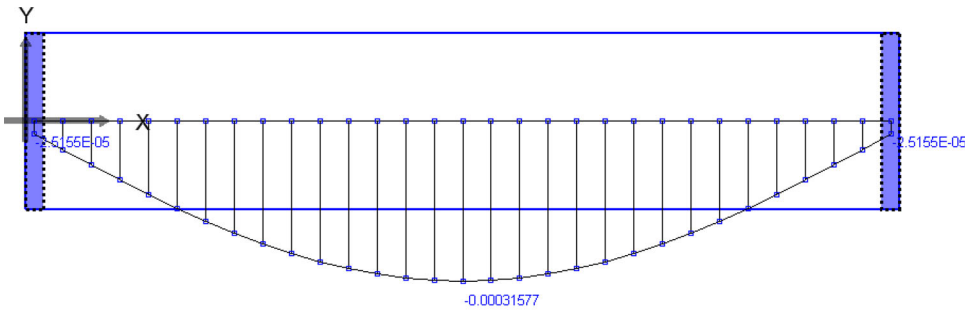

(a) Deflection (m).

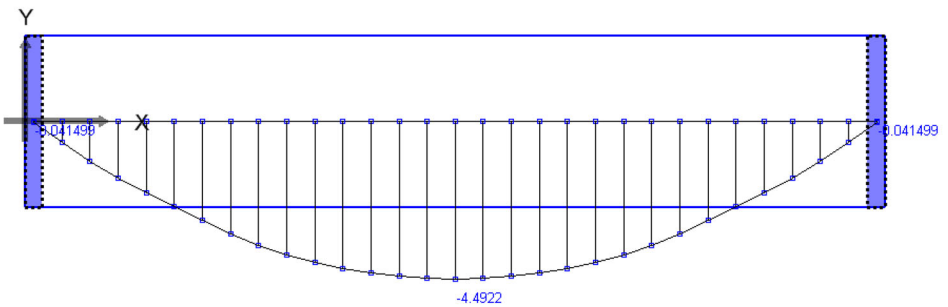

(b) Bending moment (m.t).

Fig. 6 Deflection and bending moment distribution under the slab own weight along the slab center line in the simply supported slab considered in Sect. 4.1

Table 1 Comparison of central deflection against analytical values (m)

Case description	Analytical equation for central deflection[16]	Analytical value	Present result	Profile
Parabolic profile	$\frac{5}{48}\frac{Pe\ell^2}{EI}$	6.29E-04	6.50E-04 (Error of 3.33%)	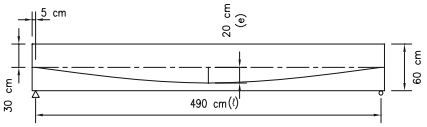
Constant eccentricity	$\frac{1}{8}\frac{Pe\ell^2}{EI}$	7.54E-04	7.61E-04 (Error of 0.93%)	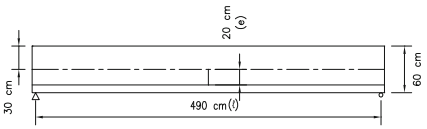
Single harping point	$\frac{(2e_c+e_e)}{24}\frac{P\ell^2}{EI}$	6.29E-04	6.46E-04 (Error of 2.70%)	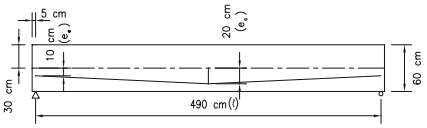
Double harping point	$\left[\frac{e_c}{8}-\frac{\beta^2}{6}(e_c-e_e)\right]\frac{P\ell^2}{EI}$	7.13E-04	7.29E-04 (Error of 2.24%)	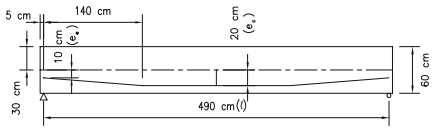

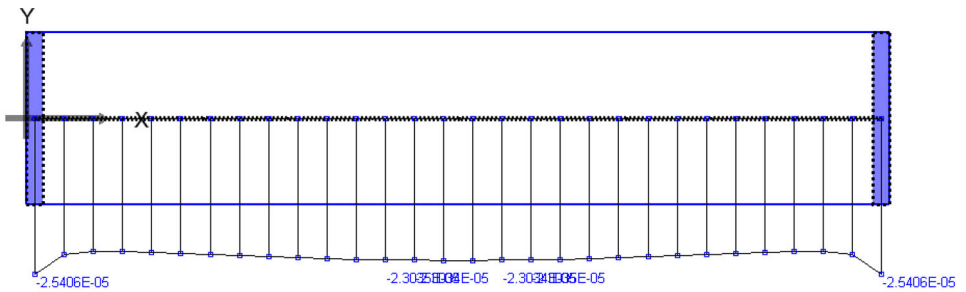

(a) Deflection (m).

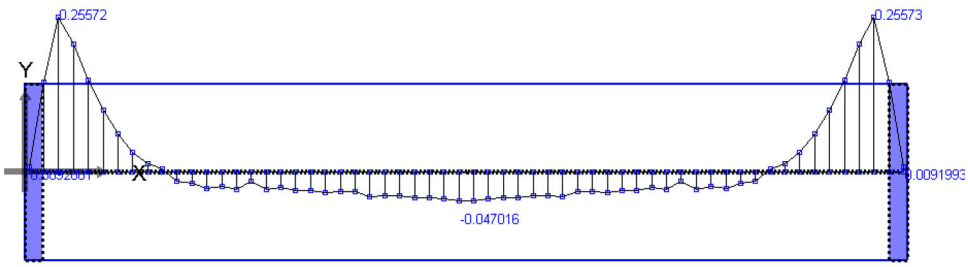

(b) Bending moment (m.t).

Fig. 7 Deflection and bending moment distributions under the slab own weight plus the balancing force prestressing cable along the slab center line in the simply supported slab considered in Sect. 4.1

equal to the balancing force 23.4 tons. The cable profile and eccentricity are shown in Fig. 4. The slab is supported on two supports of 0.1 × 1.0 m in cross section and 1.5 m in height as shown in Fig. 4. The slab boundary is modeled (see Fig. 5) using 16 boundary elements. A simply supported boundary condition is employed. Such conditions are simulated using two column support of 1.0 × 0.1 m with zero rotational stiffnesses and high value of (10^{10}) for the axial stiffness. Eleven internal cells are used to represent the cable equivalent loading. The numbers of Gauss points used for integration purposes are ten. The total number of extreme

Table 2 Comparison of fixed end moments against analytical values (m.t)

Case description	Analytical equation[16]	Analytical Value	Result (%Error)	Profile
Single harping point with no end eccentricity	$M_1 = M_2 = P\frac{e}{2}$	5.00	5.03 (0.60%)	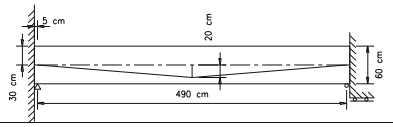
Parabolic profile with no end eccentricity	$M_1 = M_2 = P\frac{2}{3}e$	6.67	6.72 (0.75%)	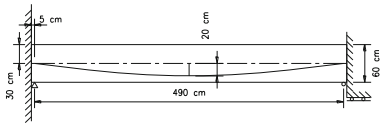
Single harping point with end eccentricity	Obtained based on stiffness analysis	M_1=0.26 M_2=1.42	M_1=0.24 (7.69%) M_2=1.40 (1.41%)	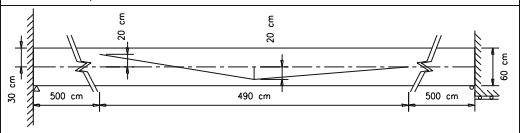

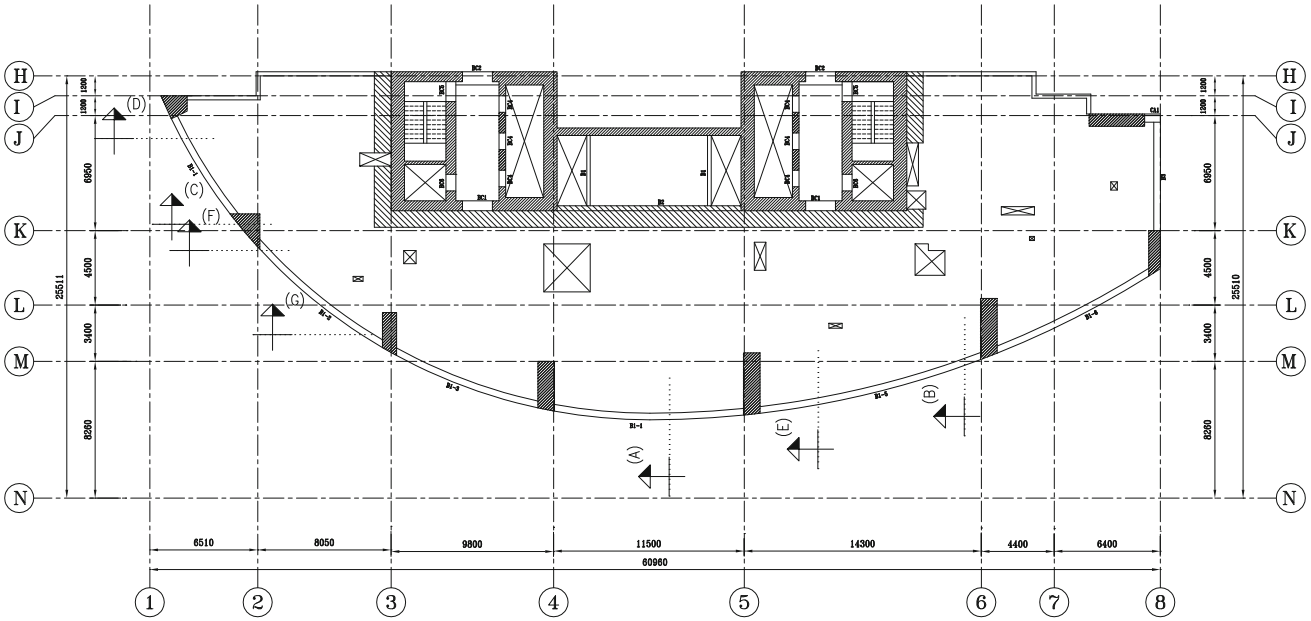

Fig. 8 The practical slab geometry and section locations (dimensions are in mm)

points is 52. The results are calculated along a strip along the cable center line.

Figure 5 demonstrates the deflection and bending moment distributions along the slab center line under its own weight only. Figure 6 demonstrates the same deflection and bending moment distributions under both own weight plus the balancing pre-stressing force. It can be seen that deflection approaches zero compared to the deflection distribution in Fig. 5. The bending moment in Fig. 6 approaches zero also; except near the end supports as such supports are not knife edge and has width of 0.1 m; therefore small negative moment is expected.

Comparison of central deflection against analytical values

The same example in Sect. 4.1 is reconsidered herein using different cable profile (see Table 1). The present boundary element results for the deflection at the mid span are shown in Table 1. It can be seen from Table 1 that the results for the central deflection are in excellent agreement with analytical values obtained from Ref. Michael and Denis (1997). The symbols used in Table 1 are: P is pre-stressing force, e, e_c are the centerline eccentricity, e_e is end eccentricity, E is modulus of elasticity, I is section moment of

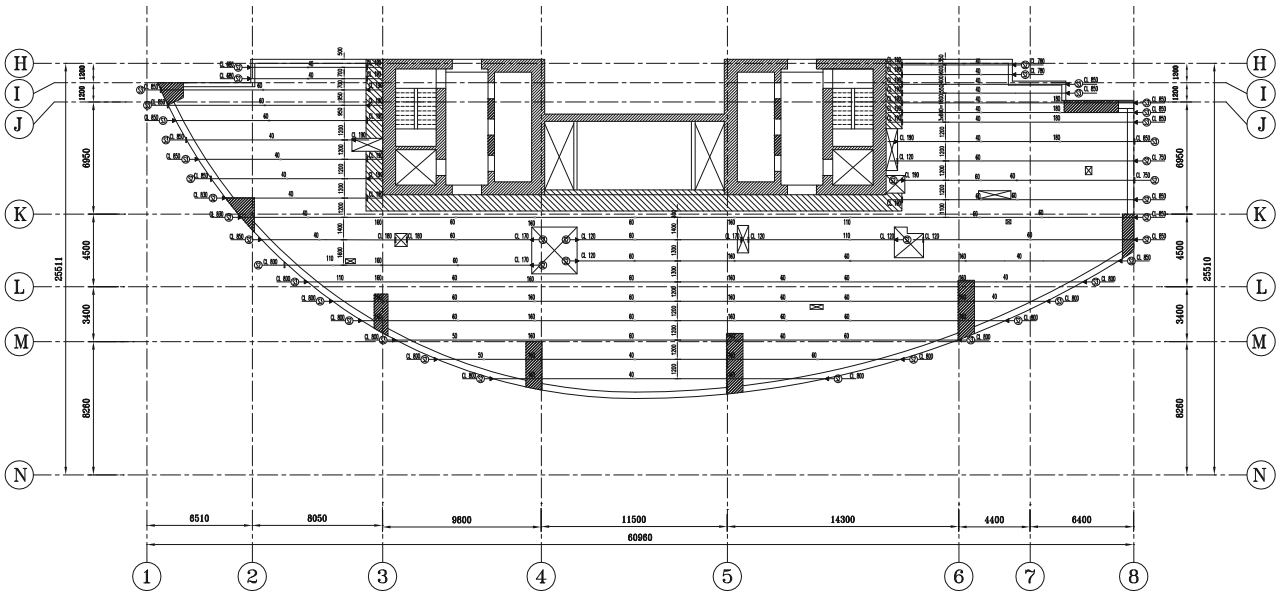

Fig. 9 Cables layout in the *X*-direction

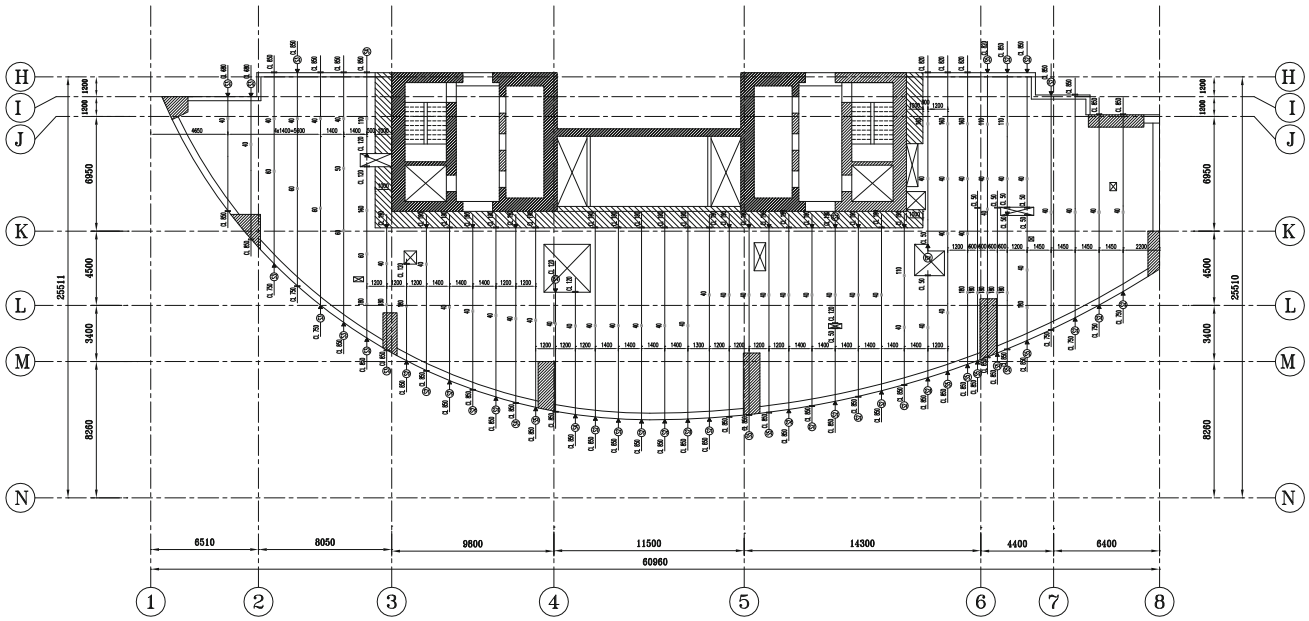

Fig. 10 Cables layout in the *Y*-direction

inertia, β is the ratio of the distance from the harping point to the beam end, to the beam length. This ratio is equal to 1.4/4.9 in the considered case (Fig. 7).

Comparison of fixed end moments against analytical values

Using the same slab in Sect. 4.1, alternative cases are considered herein to verify values of the fixed end moments. The cable profiles shown in Table 2 are considered. In this case the fixed–fixed boundary condition is employed. Such conditions are simulated within the boundary element model using the same previous columns but with very high value of (10^{10}) for the axial and the rotational stiffnesses in the two directions. The results of the proposed model fixed end moments together with the analytical values obtained from Michael and Denis (1997) are given in Table 2. It can be seen that the obtained results are in excellent agreement with analytical values. It is worth mentioning that in the last case, the end fixations are

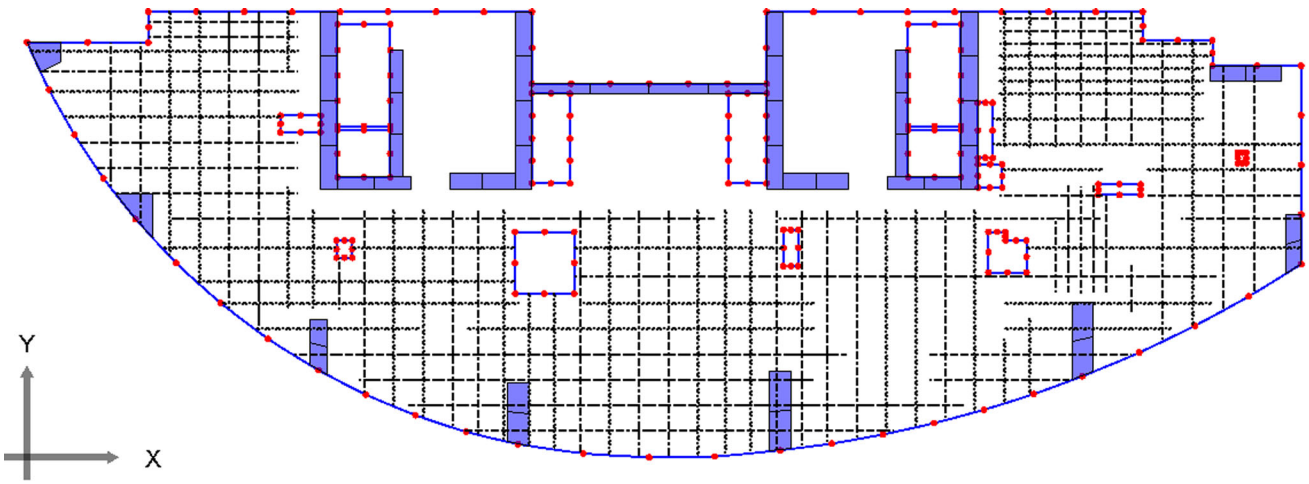

Fig. 11 The boundary element model with cable cells and support cells

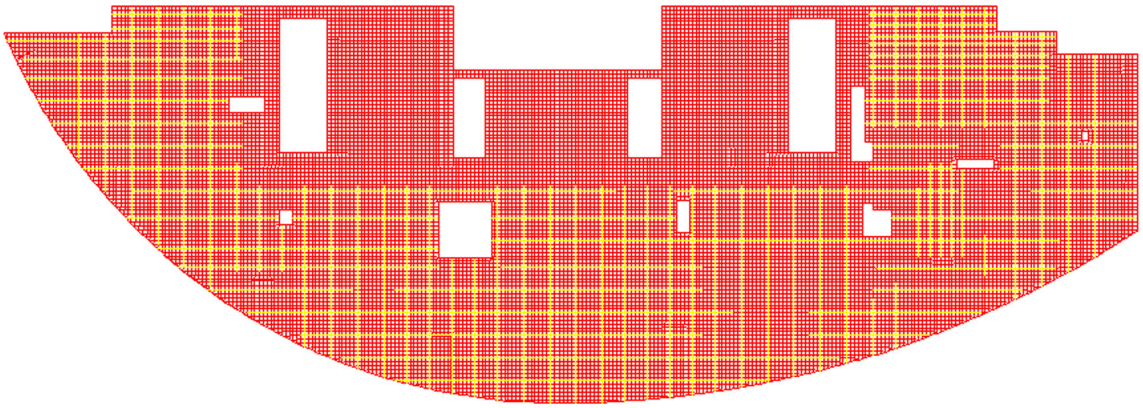

Fig. 12 The finite element model

spaced by distant 5.0 m away from the cable end to avoid the placement of the concentrated moment near the fixed column.

Practical application

The previous simple cases (in Sect. 4) verified the present formulation. In this example, the slab shown in Fig. 8 is considered. The purpose of this example is to demonstrate that the present formulation can be used as an alternative to the existing finite element based software packages. The slab has maximum dimensions of 61 × 26 m with spans about 7 to 11 m and thickness of 0.24 m. The material properties taken are $E = 2.1 \times 10^6$ t/m^2, $\nu = 0.16$. The slab is pre-stressed with cables in X & Y directions as shown in Figs. 9 and 10, respectively. Cables spacing varies from 0.6 to 1.6 m and cable force are equal to 12 ton. Cable groups are used. Each group contains 2 to 5 cables. Cable layout and eccentricity are shown in Figs. 9 and 10, respectively. The slab is supported on group of

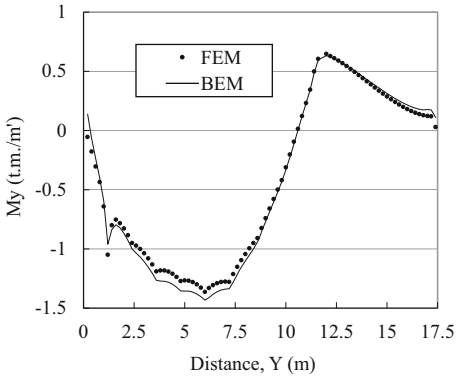

Fig. 13 Bending moment along section A (m.t)

irregular columns (cross section varies from 2 to 4 m^2) and central core as shown in Fig. 9. The floor height is 3 m.

The slab boundary is modeled using the proposed boundary element models using 159 boundary elements and 4124 internal cells are used to represent the equivalent loading of cables as shown in Fig. 11. The number of

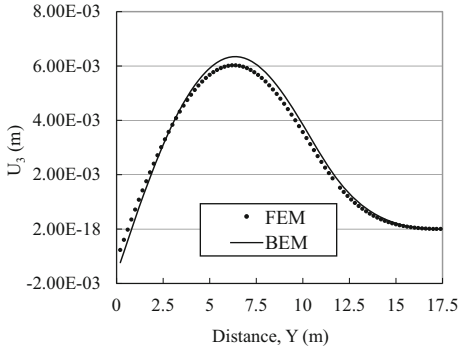

Fig. 14 Deflection along section A (m)

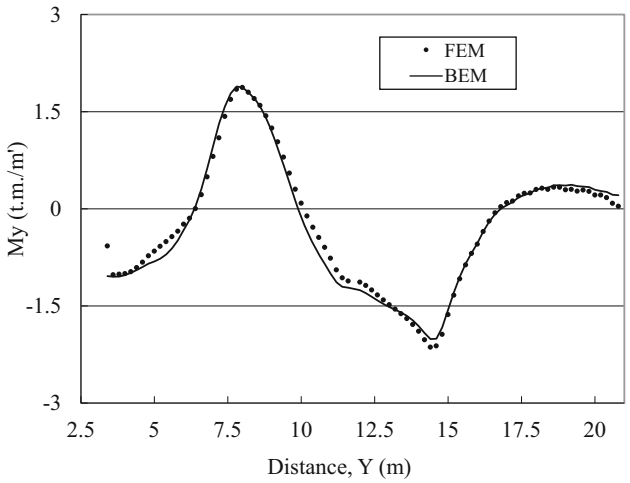

Fig. 15 Bending moment along section B (m.t)

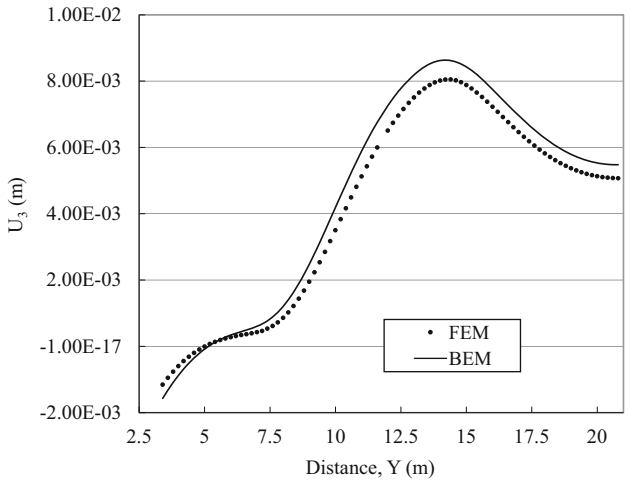

Fig. 16 Deflection along section B (m)

Gauss points used is 4. Total number of extreme points is 8787. The results are calculated along several sections using 515 internal points and internal point meshes of 1×1 m are used for contour map calculations. The

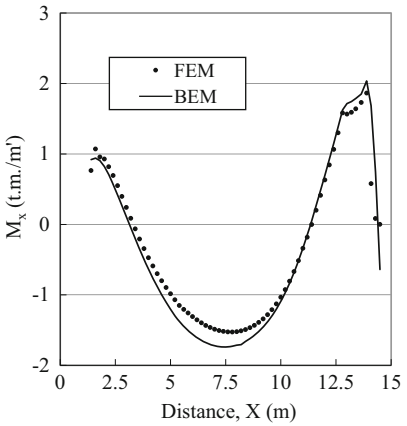

Fig. 17 Bending moment along section C (m.t)

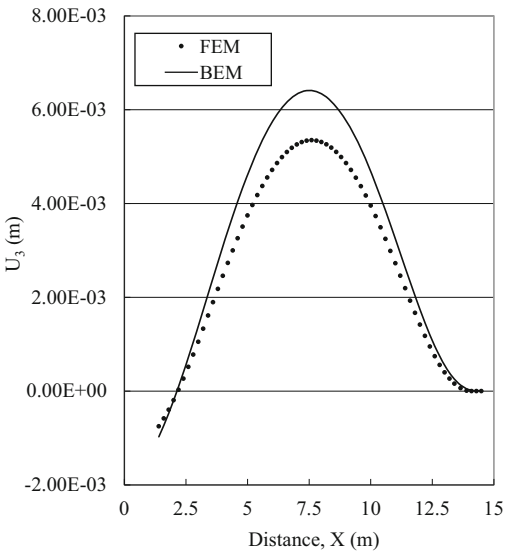

Fig. 18 Deflection along section C (m)

internal columns and cores are represented by multiple supporting cells (2 to 4 cells).

The same slab is considered using finite element analysis with 0.2×0.2 m mesh, columns are represented as 3D solids, shear walls and cores are represented using shell element. The used finite element model has 87,003 nodes and 22,098 four-node plate-bending elements as well as 48,990 solid elements as shown in Fig. 12. It has to be noted that results presented in this section will concentrate on slab results. Discussions on results for supporting elements are similar to those of slabs without pre-stressing cables which have been already considered by Rashed (2005a, b).

Figures 13, 14, 15, 16, 17, 18, 19, 20, 21, 22, 23, 24, 25 and 26 demonstrate the distribution of bending moment and deflection results along sections A, B, C, D, E, F and G in the considered slab (see Fig. 8). It can be seen that the

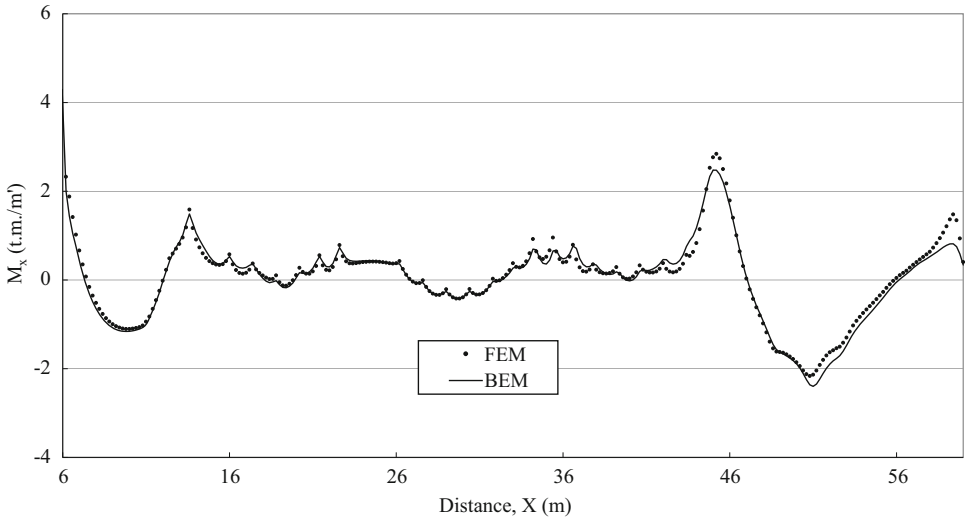

Fig. 19 Bending moment along section D (m.t)

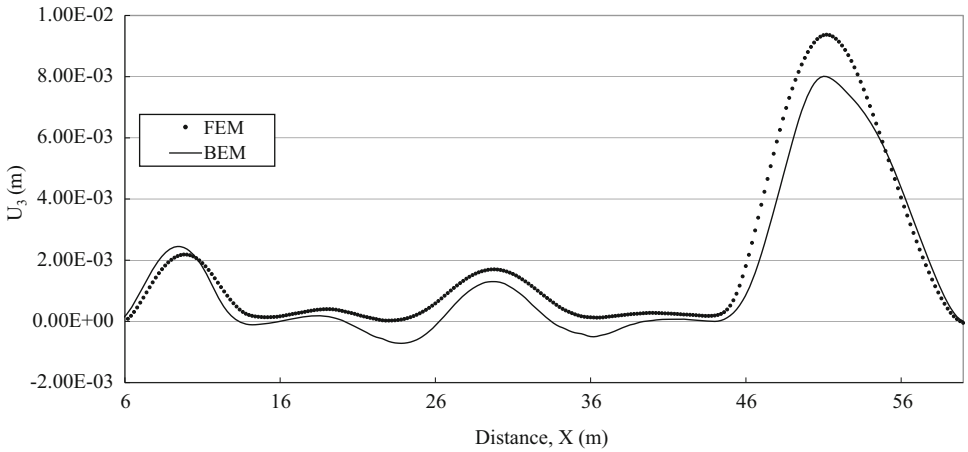

Fig. 20 Deflection along section D (m)

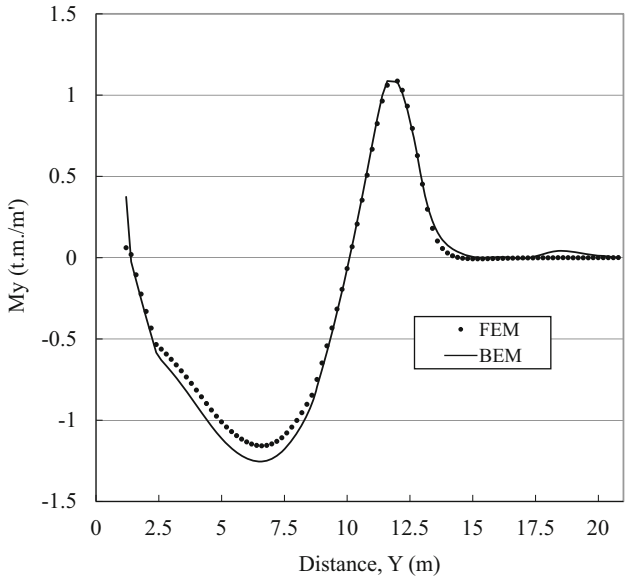

Fig. 21 Bending moment along section E (m.t)

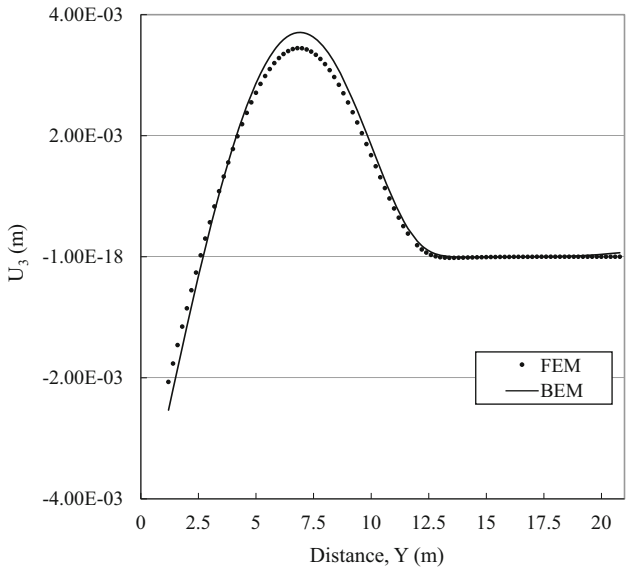

Fig. 22 Deflection along section E (m)

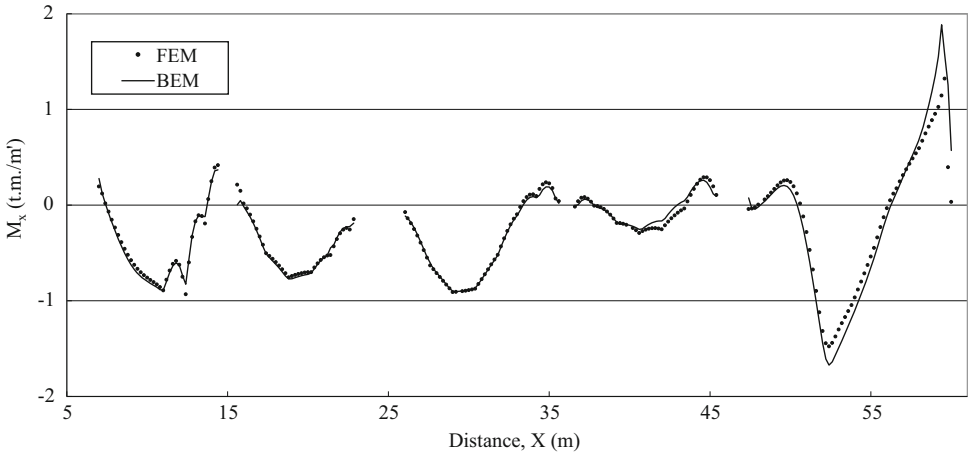

Fig. 23 Bending moment along section F (m.t)

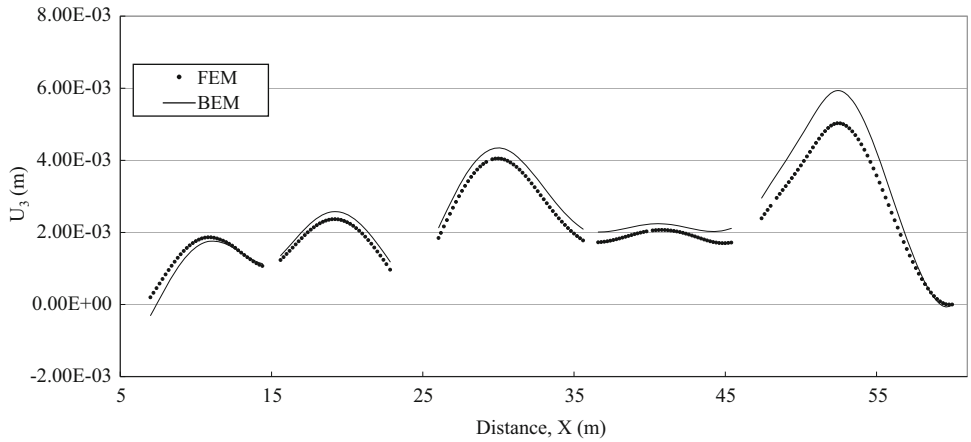

Fig. 24 Deflection along section F (m)

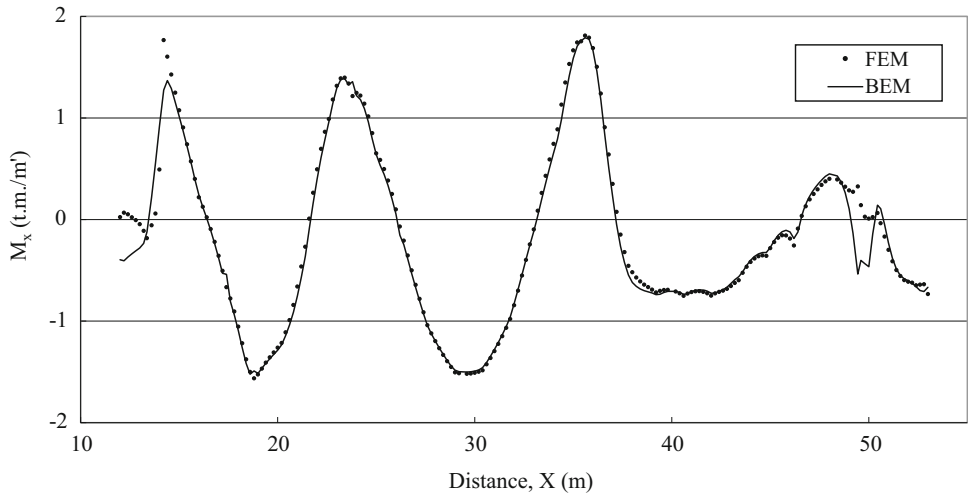

Fig. 25 Bending moment along section G (m.t)

presented formulation (BEM) results are in good agreement when compared to results obtained from finite element analysis (FEM). Figures 27, 28, 29, 30, 31 and 32 demonstrate the contour map results of bending moment and deflection, respectively. An effort is made to have as much a similar color range as possible in the two analyses

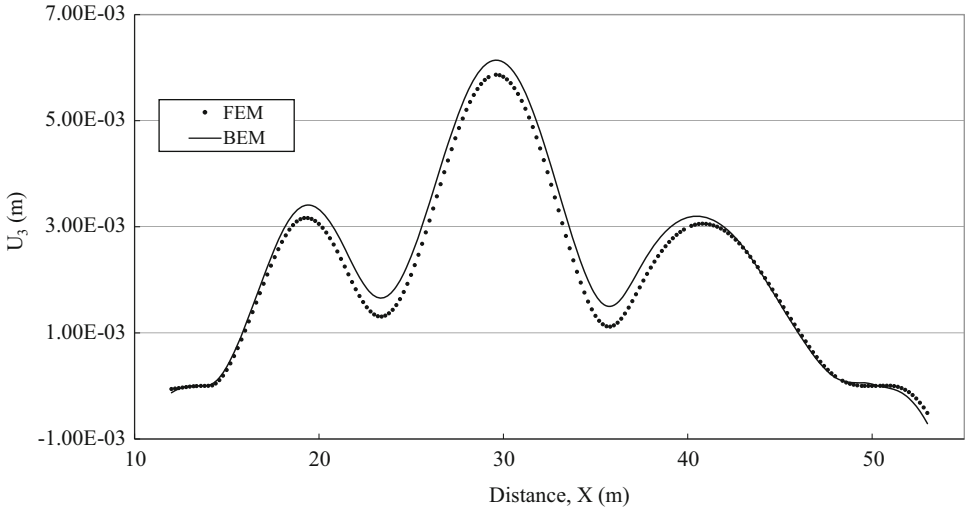

Fig. 26 Deflection along section G (m)

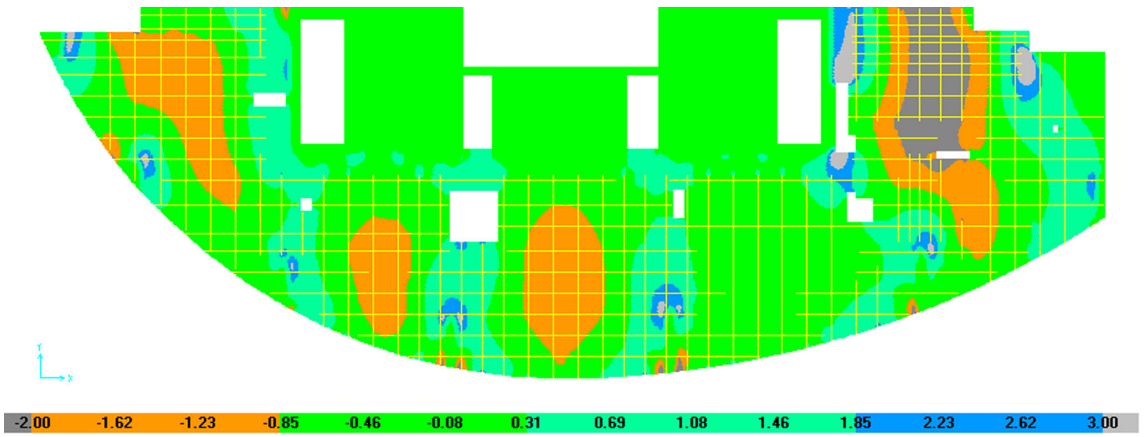

Fig. 27 Contour map for bending moment M_{xx} in the finite element model (m.t)

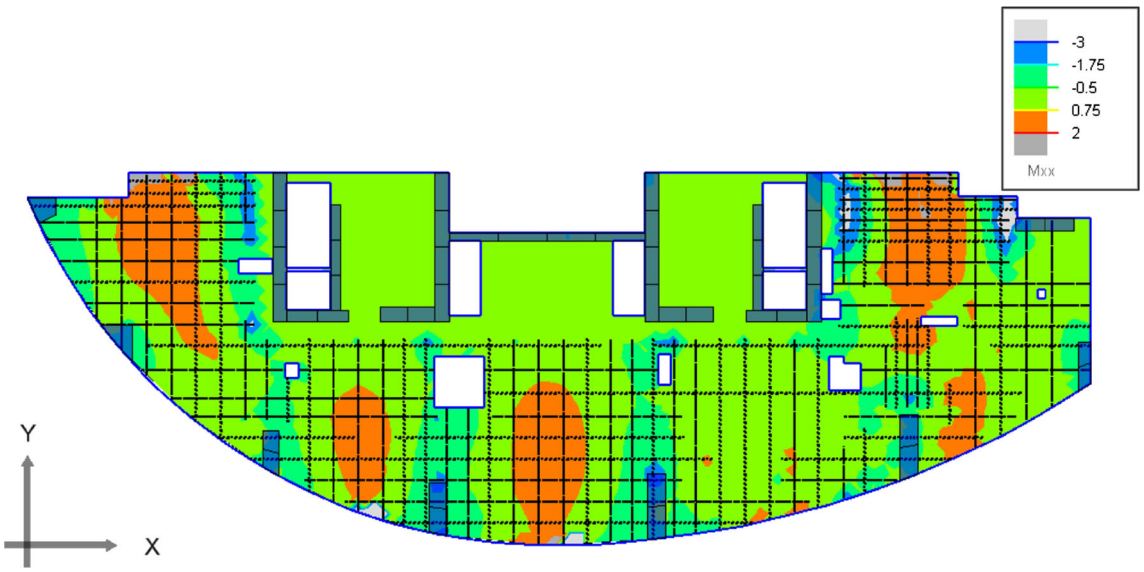

Fig. 28 Contour map for bending moment M_{xx} in the boundary element model (m.t)

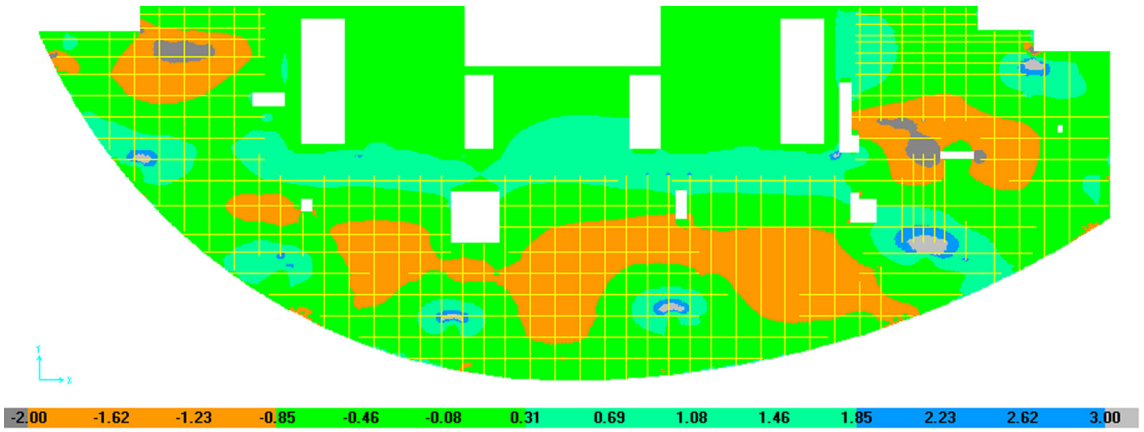

Fig. 29 Contour map for bending moment M_{yy} in the finite element model (m.t)

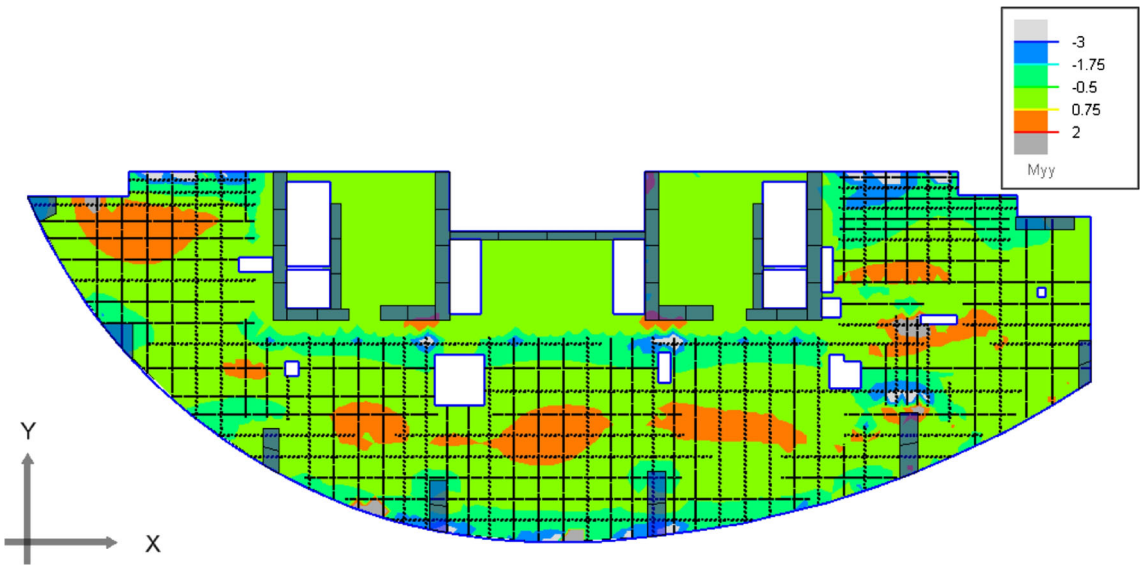

Fig. 30 Contour map for bending moment M_{yy} in the boundary element model (m.t)

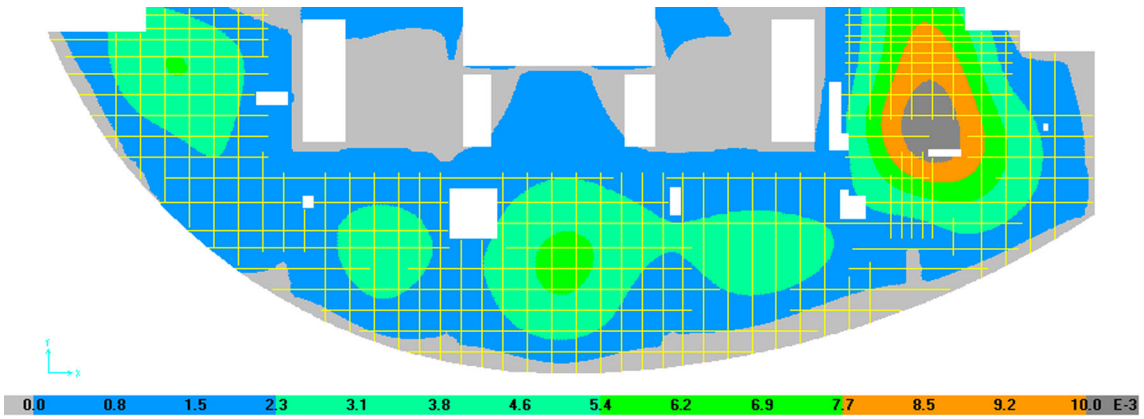

Fig. 31 Contour map for vertical deflection U_z in the finite element model (m)

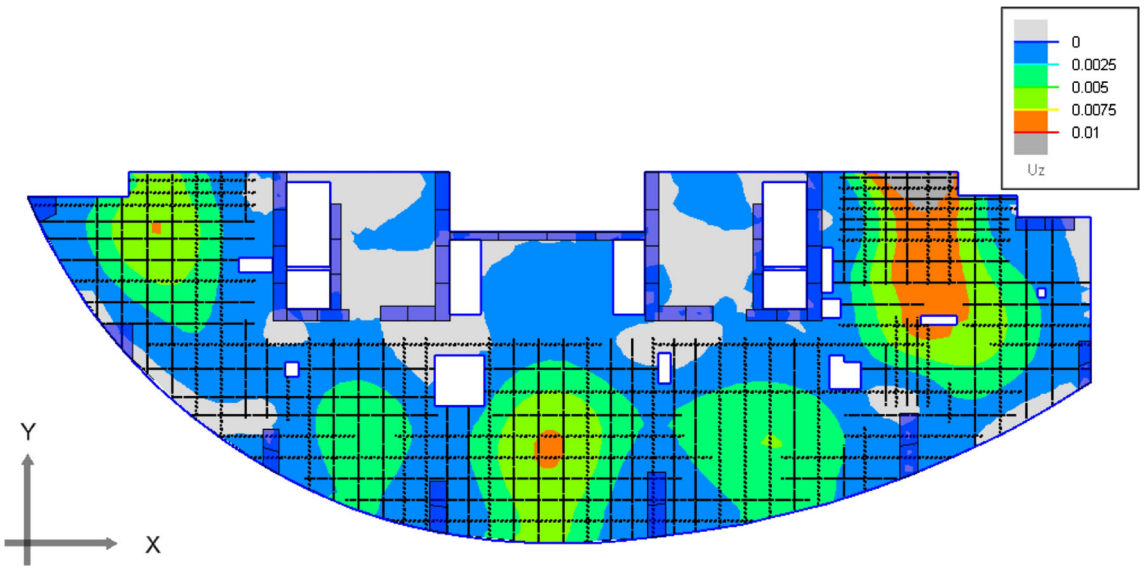

Fig. 32 Contour map for vertical deflection U_z in the boundary element model (m)

Table 3 A comparison between the present BEM and FEM results

	FEM	BEM
Time (min)	75	1 (98.67 % less in time)
Size (MB)	2530	4.5 (99.82 % less in storage)

(BEM and FEM). It can be seen that the results of the present (BEM) agree with those obtained from the (FEM) results. Table 3 demonstrates a comparison in terms of computer running time and computer storage requirements between the present (BEM) and (FEM). The superiority of the present formulation can be seen from this table.

Conclusions

The present paper developed a new boundary element formulation that account for the effect of pre-stressing cables in flat slabs. The equivalent load method is used to simulate the effect of pre-stressing cables. The formulation is automated and tested against simple cases and practical problems. The present formulation has many advantages over the existing finite element based codes in terms of data preparations, computer time and storage requirements. Analysis of pre-stressed foundation plates, punching calculations and pre-stressing losses could be easily considered using the proposed model. However, they will be considered as future research. The present method could also be regarded as a fast checking tool for results obtained from existing FEM-based software packages. It is also a promising tool for value engineering.

References

ADAPT manual (2007) ADAPT Corporation, California, USA
Berrebia CA, Telles JCF, Wrobel LC (1984) Boundary element techniques: theory and applications in engineering. Springer, Berlin, Heidelberg
Bézine G (1978) Boundary integral formulation for plate flexure with arbitrary boundary conditions. Mech Res Commun 5:197–206
Lin TY (1963) Load-balancing method for design and analysis of prestressed concrete structures. ACI J 60(6):719–742
Michael PC, Denis M (1997) Prestressed concrete structures. Response Publications, Canada
Nazief MA, Rashed YF, El-Degwy WM (2010) A BEM calculation of moment transfer parameters in slab-column connections. ACI J Struct Eng 107(2):164–169
Post tensioning manual (2000) Post-tensioning institute, 5th edn, US
Rashed YF (2005a) Boundary element modelling of flat floors under vertical loadings. Int J Numer Methods Eng 62:1606–1635
Rashed YF (2005b) A boundary/domain element method for analysis of building raft foundations. Eng Anal Bound Elem 29:859–877
Reissner E (1947) On bending of elastic plates. Quart Appl Math 5:55–68
SAFE and SAFE-PT manuals (2008) Computers and structures, Berkeley, California, USA
SAP2000 manual (2006) Computers and structures, Berkeley, California, USA
Stern M (1979) A general boundary integral formulation for the numerical solution of plate bending problems. Int J Solid Struct 15:769–782

Tottenham H (1979) The boundary element method for plates and shells. In: Banerjee PK, Butterfield R (eds) Developments in boundary elements, vol. 1, Chapter 8, pp 173–205

Vander Weeën F (1982) Application of the boundary integral equation method to Reissner's plate model. Int J Numer Methods Eng 18:1–10

Zienkiewicz OC (1977) The finite element method, 3rd edn, McGraw-Hill, New York